A box model of the Late Miocene Mediterranean Sea: Implications from combined $^{87}Sr/^{86}Sr$ and salinity data

R. P. M. Topper,[1] R. Flecker,[2] P. Th. Meijer,[1] and M. J. R. Wortel[1]

Received 7 October 2010; revised 17 June 2011; accepted 29 June 2011; published 21 September 2011.

[1] Under certain conditions the strontium isotope ratio in the water of a semi-enclosed basin is known to be sensitive to the relative size of ocean water inflow and river input. Combining Sr-isotope ratios measured in Mediterranean Late Miocene successions with data on past salinity, one can derive quantitative information on the Mediterranean hydrological budget at times before and during the Messinian Salinity Crisis (MSC). Previous studies obtained this hydrological budget by inverting the salinity and strontium data with steady state solutions to the conservation equations of salt, strontium and water. Here, we develop a box model with a time-dependent set of equations to investigate the coeval evolution of salinity and Sr ratios under different water budgets, gateway restrictions and riverine Sr characteristics. Model results are compared with the salinity and strontium ratio data from the Mediterranean. With a present-day water budget, strontium ratios in the Mediterranean never reach the observed Messinian values regardless of gateway restriction and water budget. However, a model with tripled river input, as inferred for the Late Miocene, is able to reproduce the Sr ratios observed. The onset of the MSC can be explained with a simple restriction of the gateway(s) between the Mediterranean and Atlantic. Lower Evaporite gypsum formed in a basin with less outflow to the Atlantic than modeled in previous studies because of the large Late Miocene river input. Evaporite thicknesses predicted by our model and consistent with the Messinian Sr ratios are on the low end of the thickness range inferred from seismics.

Citation: Topper, R. P. M., R. Flecker, P. Th. Meijer, and M. J. R. Wortel (2011), A box model of the Late Miocene Mediterranean Sea: Implications from combined $^{87}Sr/^{86}Sr$ and salinity data, *Paleoceanography*, *26*, PA3223, doi:10.1029/2010PA002063.

1. Introduction

[2] Almost forty years ago the presence of massive salt deposits of Messinian age was confirmed by Mediterranean DSDP drillings [*Hsü et al.*, 1973]. Ever since, these Messinian Salinity Crisis (5.96–5.32 Ma) [*Krijgsman et al.* 1999a] evaporites have been the focus of many studies. Despite this, many aspects of the MSC story remain controversial [*CIESM*, 2008].

[3] In the Late Miocene, the Betic (southern Spain) and Rifian (northern Morocco) corridors controlled connectivity between the Atlantic and the Mediterranean [*Benson et al.*, 1991]. Sediments from these gateways record periods of open exchange, restriction (due to e.g. tectonic uplift, sedimentation in the straits, tectonics, faulting and landslides) and closure [*Krijgsman et al.*, 1999b; *Betzler et al.*, 2006; *Martín et al.*, 2009; *Hüsing et al.*, 2010]. This sequence of increasing Late Miocene restriction is also reflected in changes in marine fauna and the stable oxygen and carbon isotopes of fossil carbonate in both the gateway areas and elsewhere in the Mediterranean [e.g. *Seidenkrantz et al.*, 2000; *Kouwenhoven et al.*, 2003; *Kouwenhoven and van der Zwaan*, 2006]. Other geochemical proxies also allow the reconstruction of past connectivity between the Mediterranean and the global ocean. One of these is the ratio of the strontium isotopes ($^{87}Sr/^{86}Sr$) which may be incorporated and preserved by marine organisms in their skeletal biogenic carbonate or phosphate (e.g. fish teeth, foraminiferal and ostracod shells). Authigenic marine minerals such as evaporites also preserve the $^{87}Sr/^{86}Sr$ of the water from which they precipitated.

[4] In the global ocean, strontium has a residence time of several million years with a mixing time of about 1500 years [*Broecker and Peng*, 1982; *Hodell et al.*, 1990]. This warrants the assumption of spatially uniform oceanic $^{87}Sr/^{86}Sr$ on timescales greater than 1.5 kyr. When exchange with the global ocean is limited, the $^{87}Sr/^{86}Sr$ of a marginal basin will deviate from oceanic $^{87}Sr/^{86}Sr$ values toward a ratio that reflects the Sr isotope ratio of non-oceanic inputs, principally river water and hydrothermal fluids. The Sr isotope ratio of river water reflects the geology of its catchment. Because of the predominantly granitic nature of the conti-

[1]Department of Earth Sciences, Faculty of Geosciences, Utrecht University, Utrecht, Netherlands.
[2]BRIDGE, School of Geographical Sciences, Bristol University, Bristol, UK.

0883-8305/11/2010PA002063

Table 1. Overview of Parameter Values Used for Both the Modern and Late Miocene Mediterranean

Parameter	Detail	Value	Reference
	Mediterranean Volume/Surface Area		
V_M	Present-day volume	$3682.8 \cdot 10^{12}$ m^3	
A	Present-day surface area	$2.4788 \cdot 10^{12}$ m^2	
V_M	Late Miocene volume	$3750.7 \cdot 10^{12}$ m^3	[*Meijer et al.*, 2004]
A	Late Miocene surface area	$2.4780 \cdot 10^{12}$ m^2	[*Meijer et al.*, 2004]
V_M	Messinian volume	$5736.7 \cdot 10^{12}$ m^3	[*Govers et al.*, 2009]
A	Messinian surface area	$2.6951 \cdot 10^{12}$ m^2	[*Govers et al.*, 2009]
	Present-Day Fresh Water Fluxes		
E-P	Evaporation - precipitation	0.6 m yr^{-1}	[*Mariotti et al.*, 2002]
R_{west}	River input in WMed	4250 m^3 s^{-1}	[*Meijer and Krijgsman*, 2005]
R_{east}	River input in EMed	13400 m^3 s^{-1}	[*Meijer and Krijgsman*, 2005]
	Messinian Fresh Water Fluxes		
E-P	Evaporation - precipitation	1 m yr^{-1}	[*Gladstone et al.*, 2007]
R_{west}	River input in WMed	5526.4 m^3 s^{-1}	[*Gladstone et al.*, 2007]
R_{east}	River input in EMed	36067.4 m^3 s^{-1}	[*Gladstone et al.*, 2007]
R_{Chad}	Possible discharge from Chad basin	66545.0 m^3 s^{-1}	[*Gladstone et al.*, 2007]
	Salinity		
S_A	Ocean water	35 kg m^{-3}	
S_R	River input	0 kg m^{-3}	
	Strontium Concentration		
$[Sr]_A$	Ocean water	$8 \cdot 10^{-3}$ kg m^{-3}	[*Palmer and Edmond*, 1989]
$[Sr]_{Nile}$	Nile water	$0.235 \cdot 10^{-3}$ kg m^{-3}	[*Brass*, 1976]
$[Sr]_{Rhone}$	Rhone water	$0.520 \cdot 10^{-3}$ kg m^{-3}	[*Albarède and Michard*, 1987]
$[Sr]_R$	Average Rhone and Nile water	$0.3 \cdot 10^{-3}$ kg m^{-3}	
	Strontium Isotope Ratios		
$^{87}Sr/^{86}Sr_A$	Ocean water at present	0.709175	[*McArthur et al.*, 2001]
$^{87}Sr/^{86}Sr_A$	Average during MSC	0.709006	[*McArthur et al.*, 2001]
$^{87}Sr/^{86}Sr_{Mesozoic}$	Mesozoic ocean water	0.7068–0.7084	[*McArthur et al.*, 2001]
$^{87}Sr/^{86}Sr_{Hydrothermal}$	Hydrothermal activity	~0.703	[*Palmer and Edmond*, 1989]
$^{87}Sr/^{86}Sr_{River}$	Global average river water	0.7119	[*Palmer and Edmond*, 1989]
$^{87}Sr/^{86}Sr_{Nile}$	Nile water	0.7060	[*Brass*, 1976]
$^{87}Sr/^{86}Sr_{Rhone}$	Rhone water	0.708719	[*Albarède and Michard*, 1987]
$^{87}Sr/^{86}Sr_R$	Average Rhone and Nile water	0.707427	

nental crust, this typically results in river water having higher $^{87}Sr/^{86}Sr$ than present-day ocean values (Table 1). The Mediterranean is unusual in having a northern catchment dominated by Mesozoic carbonate, which has a $^{87}Sr/^{86}Sr$ derived from the relatively low oceanic values in the Mesozoic, and a southern source (the Nile) that drains basalts which have a very low $^{87}Sr/^{86}Sr$ reflecting their mantle origin (Table 1).

[5] Many authors have used an approach based on these principles to study marginal basin restriction and local influences on $^{87}Sr/^{86}Sr$ [*McCullogh and Dekker*, 1989; *Vasiliev et al.*, 2010; *Matano et al.*, 2005; *Lugli et al.*, 2007; *Müller and Mueller*, 1991; *Müller et al.*, 1990; *Keogh and Butler*, 1999]. $^{87}Sr/^{86}Sr$ has also been used as a paleosalinity proxy in lagoonal settings where $^{87}Sr/^{86}Sr$ is assumed to be a result of simple river-ocean mixing [e.g., *Reinhardt et al.*, 1998]. Because salinity in marginal basins is also a function of evaporation, $^{87}Sr/^{86}Sr$ cannot be used as a paleosalinity tool particularly at latitudes where evaporation exceeds precipitation. However, the combination of $^{87}Sr/^{86}Sr$ data with salinity can be used to examine the hydrological budget of the basin. *Flecker et al.* [2002] were the first to recognize the role of the atmospheric fluxes (evaporation and precipitation) in determining the $^{87}Sr/^{86}Sr$ - salinity relationship and applied this to the Mediterranean to derive relative changes in the Atlantic inflow and outflow from combined $^{87}Sr/^{86}Sr$ and salinity data.

[6] The objectives of this paper are twofold: (1) a sensitivity study and (2) application of the model to the Late Miocene Mediterranean. The sensitivity study, the subject of section 4, uses a newly developed box model incorporating $^{87}Sr/^{86}Sr$ as a passive tracer to provide more insight in the interpretation of Late Miocene combined salinity-$^{87}Sr/^{86}Sr$ data. We explore the influence of fresh water budget, gateway restriction, strontium characteristics of the input fluxes, and basin size/volume, on the co-evolution of $^{87}Sr/^{86}Sr$ and salinity values in the Mediterranean. While *Flecker et al.* [2002] used steady state solutions to the equations that express conservation of Sr isotopes, salt and water, we model the evolution of these parameters with a time-dependent set of equations. This is a significant advance since it allows examination of transient behavior and appraisal of the validity of the assumption of a steady state, inherent to the analysis of *Flecker et al.* [2002] and *Flecker and Ellam* [2006]. Moreover, we examine the role of the various fluxes individually, rather than in the form of dimensionless combinations of these fluxes as adopted in this previous work. In section 5, we apply the knowledge gained to the Late Miocene Mediterranean. Addressed are the significance of $^{87}Sr/^{86}Sr$ data from sub-basins prior to

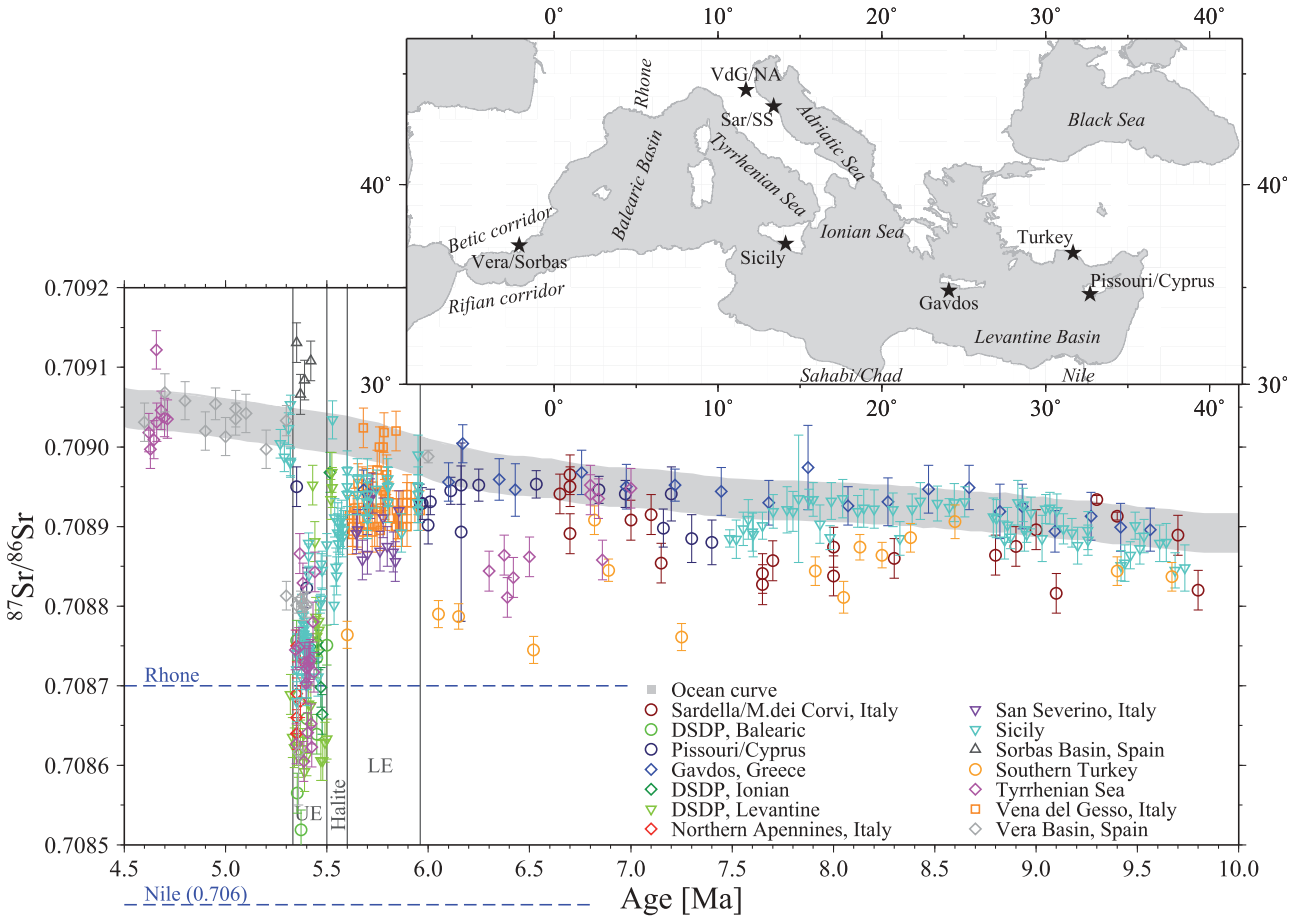

Figure 1. Late Miocene-Pliocene $^{87}Sr/^{86}Sr$ data from the Mediterranean: Sardella/Monte dei Corvi (Sar) [*Montanari et al.*, 1997]; Balearic, Ionian and Levantine basins [*Müller and Mueller*, 1991; *McCullogh and Dekker*, 1989]; Pissouri/Cyprus [*Flecker and Ellam*, 2006]; Gavdos, Greece [*Flecker et al.*, 2002]; Northern Apennines (NA) [*Bassetti et al.*, 2004]; San Severino (SS) [*Müller and Mueller*, 1991]; Sicily [*Sprovieri et al.*, 2003; *Müller and Mueller*, 1991; *McKenzie et al.*, 1988]; Sorbas Basin [*McCullogh and Dekker*, 1989]; Southern Turkey [*Flecker and Ellam*, 1999]; Tyrrhenian Sea [*Müller and Mueller*, 1991; *Müller et al.*, 1990]; Vena del Gesso (VdG) [*Lugli et al.*, 2007]; Vera Basin [*Müller*, 1993; *Fortuin et al.*, 1995]; and the global ocean $^{87}Sr/^{86}Sr$ curve [*McArthur et al.*, 2001]. Ages are corrected to fit the *CIESM* [2008] age model. When error bars are not given in the reference, error bars for the data are ±0.000025, similar to the global ocean curve.

the MSC, whether simple gateway restriction can be the mechanism of the MSC onset, and how much evaporite can be deposited during the MSC.

2. The Late Miocene $^{87}Sr/^{86}Sr$-Curve

[7] The Late Miocene-Pliocene $^{87}Sr/^{86}Sr$ data set (Figure 1), compiled by *Flecker et al.* [2002], has been extended to include recently published data, and ages are corrected to fit the *CIESM* [2008] age model. It includes data from evaporites, bulk carbonate, forams (benthic and planktic), ostracods, bivalves and fish teeth. Assessing whether the Sr isotope data have been modified by diagenetic alteration is clearly important. Early Sr measurements on foraminifera that deviated from coeval ocean water Sr isotope ratios were considered to be indicative of diagenetically altered carbonate [e.g., *Müller et al.*, 1990]. More recently however, this assumption has been challenged [*Flecker and Ellam*, 1999] and although some diagenetic alteration is likely, the evidence to suggest that this has changed the Sr isotope ratio significantly is not at all robust. We have therefore included all relevant published $^{87}Sr/^{86}Sr$ datain the data set considered here. A more extensive discussion of diagenetic alteration can be found in Text S1 in the auxiliary material.[1]

[8] Data from pre-MSC sections can be subdivided in two groups; data from central Mediterranean basins are generally within the error range of coeval ocean water, while some of the data from marginal basin settings deviates significantly from the ocean water curve (Figure 1) [*McArthur et al.*, 2001]. This spatial variation in $^{87}Sr/^{86}Sr$ within the Mediterranean has been interpreted as indicating restriction of Mediterranean-Atlantic exchange allowing the development of isotopically distinct marginal sub-basins several million years before the onset of the MSC [*Flecker et al.*, 2002].

[1] Auxiliary materials are available in the HTML. doi:10.1029/2010PA002063.

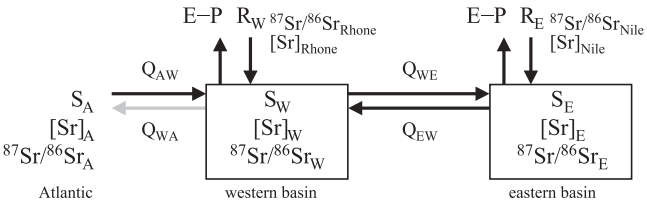

Figure 2. Diagram of the box model. The grey arrow denotes Q_{WA}, the volume flux from the western basin to the Atlantic, which is zero during completely blocked outflow; Q_{AW}, volume flux from the Atlantic to the western basin; Q_{WE}, volume flux from the western to the eastern basin; Q_{EW}, volume flux from the eastern to the western basin; E-P, evaporation minus precipitation, equal rates in both basins; R_W and R_E, river discharge in the two basins. Water properties of the basins, the Atlantic and river discharge use the same notation as in Table 1.

[9] Very few sections span the transition into the MSC succession. The one that does (Pissouri, Cyprus) suggests that the earliest evaporites have $^{87}Sr/^{86}Sr$ slightly lower than coeval ocean water. While there is considerable variability in the $^{87}Sr/^{86}Sr$ measured on Lower Evaporite (LE) samples, there is a trend toward values that are progressively lower than coeval oceanic values (Figure 1). During Lower Evaporite deposition (LE: 5.96–5.6 Ma) [*Krijgsman et al.*, 1999a] values throughout the Mediterranean are between oceanic values and 0.7088. The $^{87}Sr/^{86}Sr$ measured on Upper Evaporite (UE) and Lago Mare samples (5.52–5.32 Ma) [*CIESM*, 2008] are much lower still with ratios down to 0.7085. These low values are compatible with an interpretation of proportionally more riverine influx, relative to oceanic influx, from north Mediterranean rivers like the Rhone, north African rivers like the Nile and possibly the Paratethys (present-day Black Sea). At the Pliocene reflooding of the Mediterranean (5.32 Ma), strontium ratios return to oceanic values.

[10] Salinity constraints needed to derive a water budget estimate from the $^{87}Sr/^{86}Sr$ data are provided by foraminifera with a salinity tolerance of 30–40 g l^{-1} which were abundant in the period before the MSC. During LE deposition at least gypsum saturation was reached at 145 g l^{-1} (the average of the gypsum saturation range of 130–160 g/l) [*Warren*, 2006; *Flecker et al.*, 2002], and during halite deposition at least halite saturation (350 g l^{-1}) [*Warren*, 2006].

3. Model Description

[11] The model used in this study is based on the box model of *Meijer* [2006], which was developed to examine the blocked outflow scenario for the MSC. The Mediterranean Sea is represented by two boxes (Figure 2), indicative of the western and eastern basins, in which salinity, Sr concentration and $^{87}Sr/^{86}Sr$ are the unknowns. Outflow from the eastern to the western basin and from the western basin to the Atlantic is parameterized as linearly proportional to the difference in water density, which is assumed to be a function of salinity only. The factor of proportionality is the linear exchange coefficient g_{WA} in $m^3\ s^{-1}\ (g/l)^{-1}$. The exchange coefficient for the Atlantic-Mediterranean connection can be varied from values representing a large open gateway ($g_{WA} = 10^6\ m^3\ s^{-1}\ (g/l)^{-1}$) to complete closure ($g_{WA} = 0\ m^3\ s^{-1}\ (g/l)^{-1}$). The exchange coefficient for the Sicily strait is high in all our experiments, leveling out differences between the western and eastern basins. As a result our two-box model can be considered a one-box model [*Meijer*, 2006]. This is suitable for studying first order features of the $^{87}Sr/^{86}Sr$ and salinity evolution. Results with varying exchange coefficients for the Sicily strait are beyond the scope of this paper.

[12] It is through the statement for conservation of volume that the fresh water fluxes are related to inflow and outflow at the strait: inflow equals outflow plus the water deficit (E-P-R). Adopting volume conservation is justified by evidence suggesting that sea level was lower than normal only during halite deposition. The subaqueous facies of the gypsum and its presence in shallow marginal basins indicate that sea level was not much lowered at LE time [*CIESM*, 2008; *Roveri et al.*, 2008]. Also, in order to accumulate a considerable thickness of gypsum without associated halite, a return flow to the Atlantic must have existed, indicating sea level was at least above sill depth [*Krijgsman and Meijer*, 2008]. A short overview of the model equations and method of their solution is given in Appendix A.

[13] For the present-day experiment, the fresh water budget for both basins is prescribed and consists of two independent parameters: evaporation minus precipitation (E-P), which does not fractionate the Sr isotope ratio in the basin, and river discharge (R). For the present-day experiment we adopt the average atmospheric water budget from the compilation by *Mariotti et al.* [2002] and river input following *Meijer and Krijgsman* [2005]: 0.6 m/yr E-P in both basins and river discharges of 4000 and 14650 $m^3\ s^{-1}$ for the western and eastern basin respectively. River input in the model is varied around the reference value of R with a multiplication factor fR representing (1) uncertainty in the estimates of the water budget and (2) climate variation around the long term mean approximated by R. When fR = 1, river input is equal to the reference value, at fR = 1.5 it is 50% higher, and so on. For the present-day situation the variability in the water budget will be small and the fR range considered in this study (0.25–2.25) too large. However, for the Messinian, the range is realistic because of larger uncertainties. A summary of the parameters used in our model is given in Table 1.

[14] Until now, quantitative models for the MSC [e.g., *Blanc*, 2006; *Meijer and Krijgsman*, 2005; *Meijer*, 2006] used the present-day fresh water budget because Messinian water budgets were unavailable. Recently, however, a Late Miocene (8 Ma) water budget was reconstructed using an atmospheric general circulation model [*Gladstone et al.*, 2007] which provides more appropriate values for our Late Miocene experiments. The budget used will exclude the discharge from Lake Chad since it was only periodically connected to a river system draining into the Mediterranean in the Late Miocene [*Griffin*, 2002, 2006; *Otero et al.*, 2009; *Paillou et al.*, 2009]. Including its discharge would make the Mediterranean water budget positive, which is clearly inappropriate for the MSC prior to the Lago Mare. However, the implications of adding Lake Chad discharge to the Mediterranean fresh water budget as well as general changes in the water budget will be elaborated on in the discussion.

[15] Although strontium isotope ratios of Late Miocene oceanic water can be reconstructed [*McArthur et al.*, 2001],

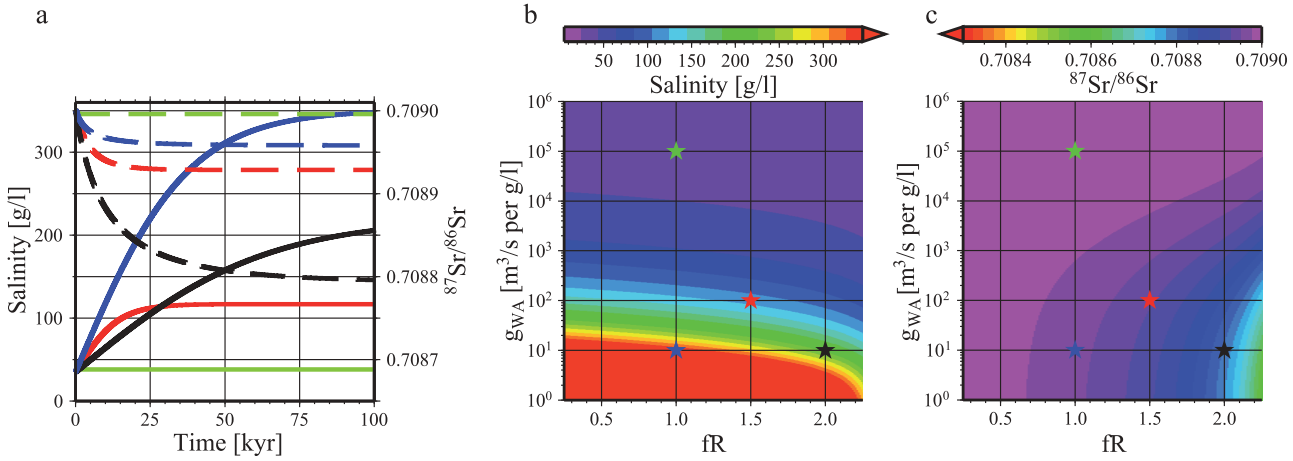

Figure 3. (a) Shows the time evolution of salinity (solid lines) and $^{87}Sr/^{86}Sr$ (dashed lines) for the first 100 kyr of experiments with a present-day water budget and initial salinity, Sr concentration and $^{87}Sr/^{86}Sr$ equal to the Atlantic. At the start of each experiment restriction (the linear exchange coefficient, g_{WA}) and river discharge (fR) are set to: fR = 1 and $g_{WA} = 10^5$ (green), this is similar to the present-day situation; fR = 1 and $g_{WA} = 10^1$ (blue), more restricted exchange than today, but not entirely closed; fR = 1.5 and $g_{WA} = 10^2$ (red), more restricted exchange than today with half as much river discharge as today; and fR = 2 and $g_{WA} = 10^1$ (black), twice as much river discharge with more restricted exchange than today. The final values of S and $^{87}Sr/^{86}Sr$ obtained when these model experiments reached a steady state are indicated on Figures 3b and 3c with stars for each of the combinations of fR and g_{WA}. Diagrams show (b) salinity and (c) strontium ratio as a function of river discharge (R) and the Atlantic exchange coefficient g_{WA}. R is expressed as amultiplier (fR) of the reference value which is defined as the present-day discharge (Table 1). Note the vertical logarithmic scale. Note that the color scales for salinity and strontium ratio are open at: the high end and the low end, respectively. Every value higher/lower than the maximum/minimum of the color scale is given the color of the maximum/minimum.

Late Miocene river values are unknown. We therefore follow [*Flecker et al.*, 2002] and use the present-day values as a first order approximation (Table 1). Sensitivity of the results to this choice will be examined.

[16] Salt precipitation is enabled in our box model with an adapted version of the equations used by *Krijgsman and Meijer* [2008]. The salinity tracked in the model is the sum of all dissolved salts in seawater with a composition as given in the work by *Leeder* [1999]. Gypsum saturation is reached when the salinity of the Mediterranean reaches four to five times the concentration of seawater (≈145 g/l) [*Warren*, 2006]. Only a fraction (3.6%) of all salts can precipitate as gypsum. This fraction is substracted from the total salt mass in the Mediterranean and converted to a gypsum layer of uniform thickness over the whole water-covered area with a characteristic density of 2300 kg m^{-3}. All $CaSO_4$ received by the basin subsequently is immediately deposited as gypsum. However, salinity continues to increase since only a fraction of all salt is precipitated. At halite saturation, 350 g/l, the same process repeats for halite (NaCl, 2200 kg m^{-3}).

4. Model Analysis

[17] In sections 4.1 and 4.2 we systematically explore salinity and $^{87}Sr/^{86}Sr$ as a function of river discharge, evaporation rate and restriction of the Atlantic gateway. The model is first set up to represent the present-day Mediterranean and thereafter the Late Miocene Mediterranean. For the Late Miocene configuration we will examine how the results are affected by changes in river water characteristics and basin size, and consider the time to equilibrium.

4.1. The Present-Day Mediterranean

[18] To illustrate the basics of the model, Figure 3a shows salinity and $^{87}Sr/^{86}Sr$ as a function of time after restriction for different restrictions and river discharges (fR scenarios). After a gateway restriction, the salinity in the Mediterranean increases to comply with salt conservation at the gateway ($Q_{AW} \times S_A = Q_{WA} \times S_M$). This salinity increase is never instantaneous; it takes the Mediterranean time to reach a new salinity equilibrium because additional salt only enters the Mediterranean through Atlantic inflow. Water volume conservation dictates that the volume of Atlantic inflow is equal to the sum of outflow and the net fresh water budget (E-P-R). Assuming E-P-R is positive, when river discharge is high and/or evaporation low, the fresh water deficit is small and the Atlantic inflow is small. With severe gateway restriction, outflow is low and the Atlantic inflow is small again. In both cases, the supply of salt to the Mediterranean is low and salinity increases slowly. The opposite is also true; salinity increases quickly when E-P-R is high and/or the gateways are large. After restriction, the volume of outflow (Q_{WA}) decreases in percentage terms more strongly than the inflow (Q_{AW}) because inflow is the sum of outflow and a constant term to balance E-P-R. This results in an increase in the salinity of both the Mediterranean and its outflow, which persists until the salt outflux is raised to the

same quantity as is supplied by inflow (salt conservation). At this point, steady state salinity is achieved in the Mediterranean.

[19] Figure 3 also shows that $^{87}Sr/^{86}Sr$ values deviate from Atlantic values when river input becomes more important relative to Atlantic inflow. Large river discharge and strong restriction of the gateways both increase the proportion of riverine $^{87}Sr/^{86}Sr$ that contributes to the Mediterranean value, leading to lower $^{87}Sr/^{86}Sr$ of Mediterranean water. Similar to salinity, $^{87}Sr/^{86}Sr$ reaches a new steady state quickly when the gateway is unrestricted (green curves in Figure 3a) and E-P-R is large (low fR), and more slowly when gateways are restricted (blue curves) and E-P-R is closer to zero (red and black curves).

[20] In Figures 3b and 3c, rather than the time evolution of salinity and $^{87}Sr/^{86}Sr$, we show the steady state results of a series of experiments in which gateway restriction and river discharge have been varied systematically in the same way as in Figure 3a. The modern $^{87}Sr/^{86}Sr$ value of the Mediterranean, which is equal to the Atlantic value, is reproduced by our model at fR = 1.0 and $Q_{WA} \sim 0.7$ Sv (Figure 3c). The present-day water budget, as used in this model, has a large water deficit without Atlantic inflow because it is dominated by the evaporative flux (E-P), which is approximately three times the river input (Table 1). This results in a large E-P-R over the whole fR range and a strong increase in salinity with increasing restriction (Figure 3b).

[21] Only when river input is at least 50% of the total inflow can deviations from the Atlantic $^{87}Sr/^{86}Sr$ value be measured [*Flecker et al.*, 2002]. With the present-day water budget and the wide range of modern river inputs, $^{87}Sr/^{86}Sr$ values only deviate measurably from the Atlantic value at high fR and significant gateway restriction. To explain the 0.001–0.004 deviations characterizing the Late Miocene (Figure 1) with this water budget, fR and gateway restriction must have been continuously high. The corresponding salinity, however, does not agree with the inferred Late Miocene salinity record.

[22] Varying f(E-P) instead of fR, while keeping all other parameters equal, gives almost a mirror image of Figure 3b. However, because changes in f(E-P) represent larger changes in flux volumes than fR, only extreme and unrealistic changes in E-P result in measurable deviations from Atlantic $^{87}Sr/^{86}Sr$ values. Although this could explain the $^{87}Sr/^{86}Sr$ values observed for the MSC, the change in evaporation required to explain the entire MSC record is too extreme to be realistic.

4.2. The Late Miocene Mediterranean

[23] The Late Miocene river discharge values used in our model are 1.3 times modern discharge for the western basin, 2.7 times modern eastern basin discharge and 2.4 times the modern discharge for the entire Mediterranean (Table 1) [cf. *Gladstone et al.*, 2007, Table 2]. The E-P we use is also derived from *Gladstone et al.* [2007] and is 1 m/yr. In Figure 4, at fR = 1.89 and f(E-P) = 0.53 the change from negative to positive (R-(E-P) > 0) water budget in the Mediterranean is visible. This was not seen in the present-day experiments (Figure 3) because of the relatively low river input. Moving along any line of constant g_{WA} in Figure 4a from low to high river input (left to right) in the negative water budget area, Mediterranean salinity decreases. Moving from high to low evaporation (right to left) with constant exchange coefficient, also results in reducing salinity (Figure 4d). The decrease in Mediterranean salinity reduces the salinity difference between Atlantic and Mediterranean water and this limits Mediterranean–Atlantic outflow (Figure 4c and 4f) because, in our model, we have parameterized outflow as being linearly proportional to the difference in water density which we assume to be entirely driven by salinity. Also, as the relative importance of Atlantic inflow decreases relative to the more substantial Late Miocene river input (Figure 4), the $^{87}Sr/^{86}Sr$ of Mediterranean water deviates significantly from Atlantic ratios (Figure 4b). When E-P and R balance each other exactly (fR = 1.89), the Mediterranean eventually reaches a $^{87}Sr/^{86}Sr$ close to the combined river input (Figure 4b and Table 1). Under these specific circumstances, however, salinity stabilizes at Atlantic concentrations (Figure 4a and 4d) since outflow to the Atlantic ceases when the salinity-driven density difference is zero ($S_W - S_A = 0$ in equation (A1)) and is then maintained by an exactly equal freshwater flux (R-(E-P) = 0).

[24] Figure 4 assumes constant R or constant E-P, but in reality, climate change will vary R and E-P at the same time. Because 1 m/yr is the upper limit of Late Miocene Mediterranean E-P estimates, E-P is lowered to 0.75 and 0.50 m/yr in Figure S1 in the auxiliary material. The most noticeable difference between Figures 4 and S1 is the shift of both salinity and $^{87}Sr/^{86}Sr$ patterns along the fR axis, caused by the changing river discharge to E-P ratio. Reducing E-P brings the vertical line representing a zero water budget toward lower fR. Also, the relative sizes of R and Atlantic inflow ($Q_{AW} = Q_{WA} + E - P - R$) change when E-P is reduced, because less Atlantic inflow is required to maintain constant Mediterranean volume when the evaporative flux is reduced, while R is unchanged. Therefore, when f(E-P) is reduced the Mediterranean becomes more sensitive to changes in fR and a smaller increase in R is needed at low E-P for a specific deviation from Atlantic $^{87}Sr/^{86}Sr$.

4.2.1. Strontium Characteristics of River Water

[25] The water budget is not the only parameter in the model which can have a pronounced influence on the coupled behavior of $^{87}Sr/^{86}Sr$ and salinity. The riverine Sr characteristics in the previous experiments were assumed to have been similar to present-day values. This seems a reasonable assumption for Late Miocene rivers because the geological catchment of modern rivers draining into the Mediterranean has not changed significantly over this time period [*Goudie*, 2005]. However, the Late Miocene fluvial drainage also included rivers that no longer flow today, and some of these, particularly those draining North Africa west of the Nile, were substantial [*Drake et al.*, 2008; *Griffin*, 2002, 2006]. The Sr characteristics of these rivers are not known, but it is likely that including their discharge in the Mediterranean's total freshwater input, would change the overall fluvial Sr characteristics. To assess the influence of river water [Sr] and $^{87}Sr/^{86}Sr$ on steady state $^{87}Sr/^{86}Sr$ in the Mediterranean, the model was run with constant E-P (1 m/yr) and g_{WA} restricted to 10^2 $m^3/s/(g/l)$ for a wide range of riverine $^{87}Sr/^{86}Sr$ and [Sr] values (Figures 5a and 5b). The combined effect of riverine $^{87}Sr/^{86}Sr$ and [Sr] values can only be checked if fR is also constant. Figure 5c illustrates this using fR = 1. Mediterranean $^{87}Sr/^{86}Sr$ deviates further

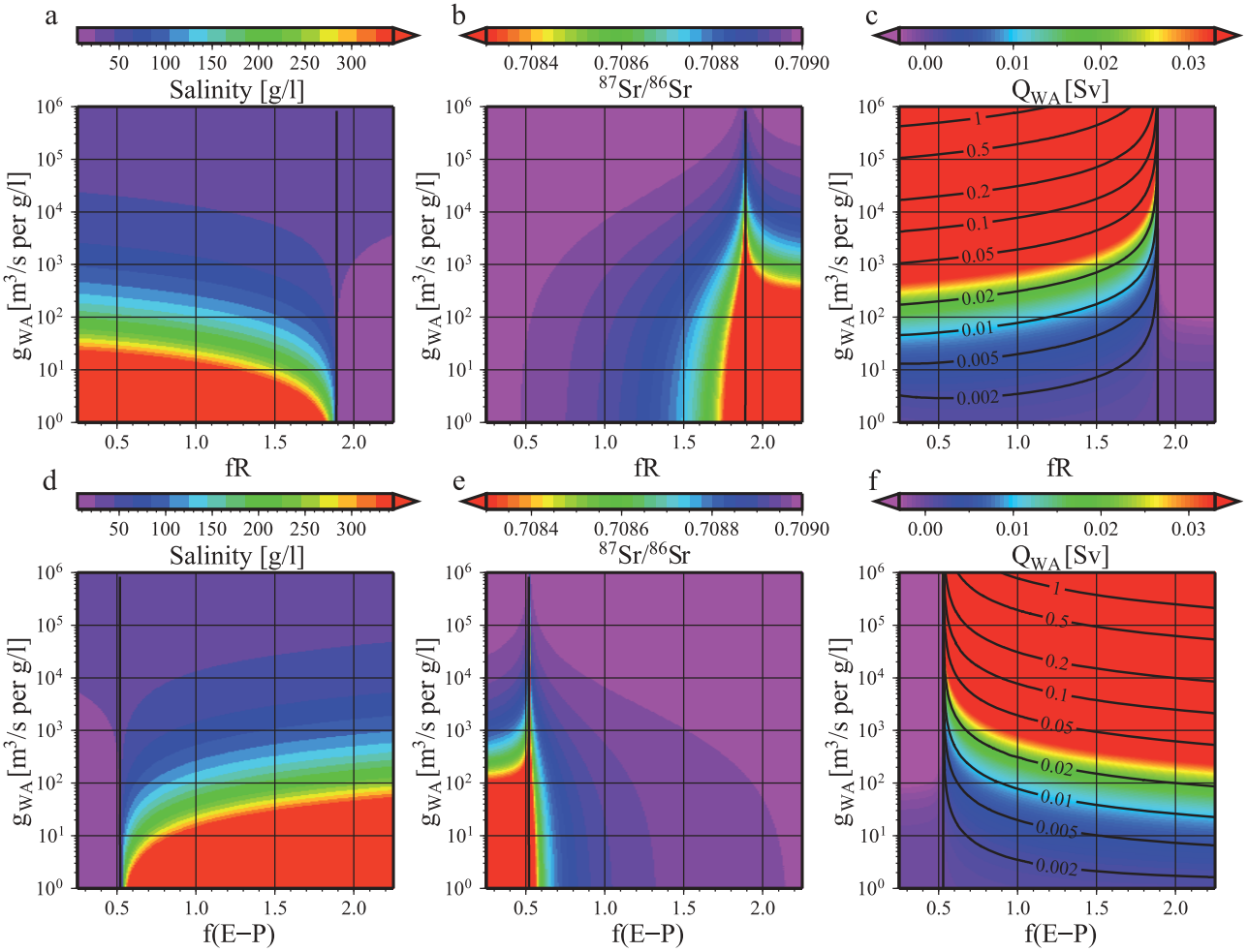

Figure 4. Diagrams show (a and d) salinity, (b and e) strontium ratio and (c and f) Mediterranean outflow to the Atlantic (Q_{WA}) as a function of river discharge (fR) (Figures 4a–4c) or evaporation-precipitation f(E-P) (Figures 4d–4f) and the Atlantic exchange coefficient g_{WA}. fR and f(E-P) are multiples of the reference values of river discharge (R) and E-P which are taken from the Late Miocene values of *Gladstone et al.* [2007]. Color scales for salinity, $^{87}Sr/^{86}Sr$ and Q_{WA} are the same as for Figure 3.

from Atlantic $^{87}Sr/^{86}Sr$ when either the [Sr] of river water increases, or when riverine $^{87}Sr/^{86}Sr$ decreases (increasing the difference between the riverine and Atlantic $^{87}Sr/^{86}Sr$). The absolute changes in Mediterranean $^{87}Sr/^{86}Sr$ are largest ($\gg$0.001) when fluvial input is approximately equal to E-P because Mediterranean $^{87}Sr/^{86}Sr$ is most strongly dependent on fluvial $^{87}Sr/^{86}Sr$ with a fresh water budget close to zero. Although the changes in Mediterranean $^{87}Sr/^{86}Sr$ shown in Figure 5 are large, their significance is limited because of the low exchange coefficient chosen (g_{WA} = 10^2 m^3/s/(g/l)). While the lowest $^{87}Sr/^{86}Sr$ is 0.70845 in Figure 5c (compared to 0.70893 at f[Sr] = 1 and d$^{87}Sr/^{86}Sr$ = 0), it is only 0.7088 (compared to 0.70898 at f[Sr] = 1 and d$^{87}Sr/^{86}Sr$ = 0) when g_{WA} is 10^4 m^3/s/(g/l). In summary, model-derived $^{87}Sr/^{86}Sr$ is most affected by uncertainty in riverine Sr characteristics when R approximates E-P and gateway restriction is severe.

4.2.2. Sensitivity to Basin Size

[26] Estimates of basin volume for the paleo-Mediterranean vary considerably from study to study (Table 1). Basin volume does not influence the steady state results for salinity and $^{87}Sr/^{86}Sr$, because at steady state there is a balance of fluxes and basin volume does not play a roll. Indeed, for dS/dt = 0 and d$^{87}Sr/^{86}Sr$/dt = 0 the solutions are independent of volume (see Appendix A). However, volume does impact the rate of change from one steady state to another since large basin volumes slow the rate of change in Sr characteristics relative to smaller basin volumes. The sensitivity of model results to basin volume is useful to examine in itself, but a small model basin is also a reasonable representation of Mediterranean sub-basins like the Adriatic and Tyrrhenian Sea.

[27] Possibly connected to a reduction in basin size, but not necessarily, is surface area which determines the total E-P flux. The combination of E-P and R determines the freshwater budget of the basin and indirectly the inflow and outflow. To assess the sensitivity of the results to basin size, we have set up a model with volume, surface area and river input at 20% of the Late Miocene values (Figure 6). With respect to the normal-sized Late Miocene model (Figure 4), the salinity response to increased gateway restriction is smaller, resulting in a larger range of restrictions without

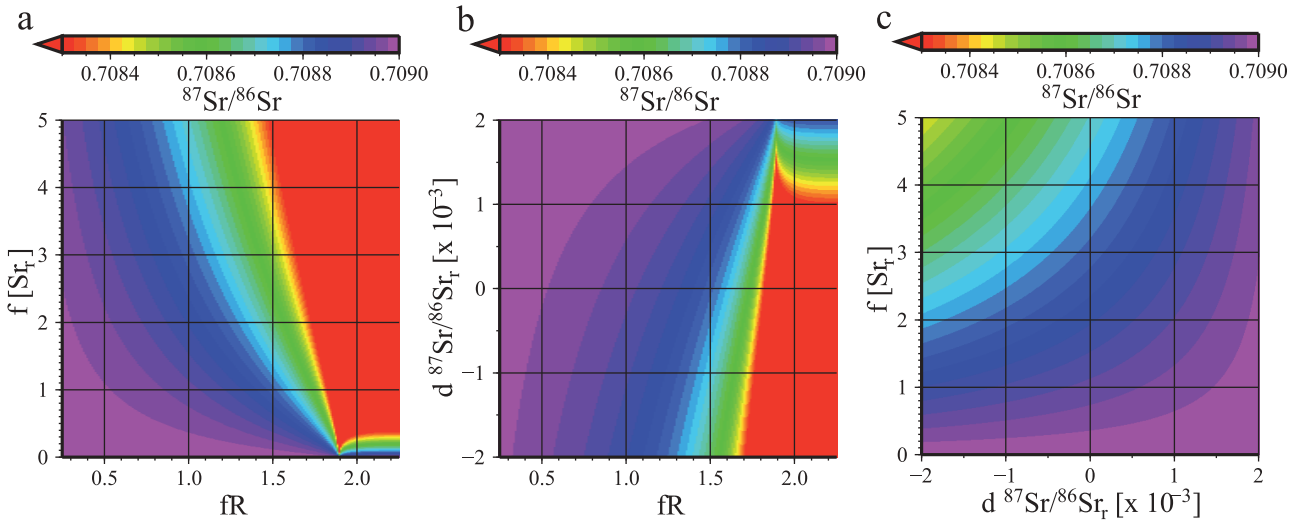

Figure 5. Sensitivity of $^{87}Sr/^{86}Sr$ to changes in the riverine water characteristics. (a) $^{87}Sr/^{86}Sr$ as a function of river discharge (fR) and riverine strontium concentration; at $f[Sr]_r = 1$ this panel intersectspanel 4b at $g_{WA} = 10^2$. (b) $^{87}Sr/^{86}Sr$ as a function of river discharge and riverine strontium ratio; at $d^{87}Sr/^{86}Sr_r = 0$ this panel intersects panel 4b at $g_{WA} = 10^2$. (c) $^{87}Sr/^{86}Sr$ as a function of riverine strontium concentration and ratio. fR and f[Sr] are multiples of the Late Miocene reference values given in Table 1. The riverine strontium ratio is expressed as a deviation of the weighted average of the riverine strontium ratio. Note that the color scale for the strontium ratio is open at the low end.

significant salinity change (Figures 6a and 4a). For a small basin E-P-R is small and consequently inflow is only slightly larger than the outflow. As shown before for changes in fR, a small difference between inflow and outflow leads to small salinity increases in the Mediterranean. Salinity only increases significantly when E-P-R becomes dominant over outflow, i.e. at significant restrictions, when the difference between inflow and outflow is relatively large (Figure 6a). The dominance of E-P-R only at significant restriction is not the only reason for the low salinities. Although exchange with a reservoir with ocean water characteristics, either the Atlantic or the pre-MSC Mediterranean, is smaller than in the normal-sized Late Miocene model, a larger percentage of the basinal water is replaced with Atlantic like water at every time step. This refreshes the buffer and suppresses large salinity increases. A reduction in basin volume alone increases its sensitivity to changes, but crucial here is the ratio of volume to exchange flow. Besides salinity, $^{87}Sr/^{86}Sr$ values also deviate less from Atlantic values, because the Sr characteristics of the small basin are

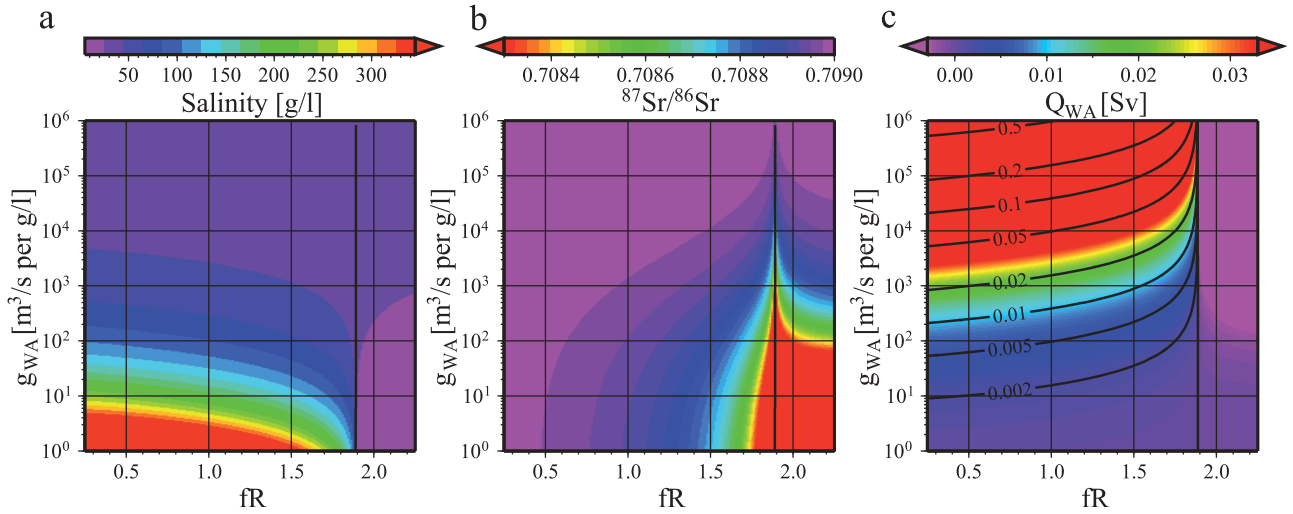

Figure 6. Diagrams show (a) salinity, (b) strontium ratio and (c) Mediterranean outflow to the Atlantic (Q_{WA}) as a function of river discharge (fR) and the Atlantic exchange coefficient g_{WA} for a box model with 1/5 of the Late Miocene Mediterranean volume and area. fR is a multiple of the reference value which is defined as 1/5 of the Late Miocene value from *Gladstone et al.* [2007]. Color scales for salinity and $^{87}Sr/^{86}Sr$ are the same as in Figure 3.

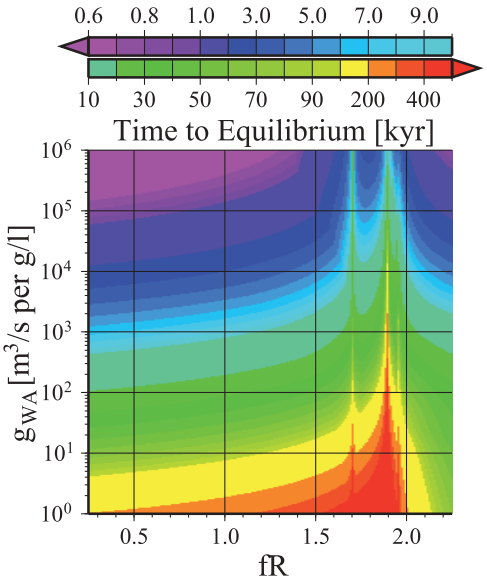

Figure 7. Time to equilibrium, starting from open marine conditions. Note that the color scale is logarithmic. See text for a more detailed explanation.

dominated by exchange with the Atlantic even when the gateway is more restricted and fR is larger. In general, small basins need more restricted exchange to reach high salinities and a fresh water budget closer to zero to obtain low $^{87}Sr/^{86}Sr$ values than larger basins.

4.3. Time to Equilibrium

[28] Previous studies examining the Late Miocene Sr-record have always described the evolution of salinity and $^{87}Sr/^{86}Sr$ in the Mediterranean as a sequence of steady states. Thus assuming for consecutive $^{87}Sr/^{86}Sr$ data points that the time to reach the new steady state is negligible. We test the validity of using steady state solutions by examining the time taken to achieve equilibrium (when salinity, [Sr], $^{87}Sr/^{86}Sr$ and the exchange fluxes don't change anymore, i.e. steady state) for each previously used combination of river input and gateway restriction (Figure 4) starting from open marine conditions (salinity: 35 g/l, [Sr]: 8 mg/l, $^{87}Sr/^{86}Sr$: 0.7090).

[29] The time taken to achieve equilibrium (t_{EQ}, Figure 7) increases with increasing restriction of Mediterranean–Atlantic exchange and when approaching a zero water budget. This behavior is best understood by considering the residence time of water elements in the Mediterranean. Longer residence time, resulting from a decrease in exchange with the Atlantic, which is caused by a smaller exchange coefficient and salinity difference, corresponds to longer t_{EQ}. In all previously presented figures substantial exchange through the Sicily Strait resulted in the parallel evolution of the eastern and western basins. In the time to equilibrium plot (Figure 7) the difference between the western and eastern basins' water budgets is clear. At fR = 1.70 the eastern basin has a zero water budget while the budget of the western basin is still negative. In the range 1.70–1.89 the exchange through the Sicily strait reverses (with surface outflow and deep inflow) because of the positive water budget in the eastern basin and the still negative water budget in the western basin and the Mediterranean basin as a whole. At fR = 1.89 the total Mediterranean water budget is zero.

[30] The important result shown in Figure 7 is that for a large range of the controlling parameters the time taken to reach equilibrium is significantly less than 50 kyr. Longer times are required only at severe restriction and when the net fresh water budget is close to zero. We therefore conclude that significant divergence from marine salinity and $^{87}Sr/^{86}Sr$ (largely exceeding the range observed in the Lower Evaporite deposits) can occur in the Mediterranean within tens of thousands of years.

5. Application to $^{87}Sr/^{86}Sr$ and Salinity Data From the Late Miocene

[31] In this section we apply the knowledge gained in the previous sections to Late Miocene data and events. First, we continue the examination of the preceding section, and take a closer look at the time to equilibrium during the MSC. Subsequently, pre-MSC sub-basin data, MSC onset and evaporite deposition are examined.

5.1. Time to Equilibrium During the MSC

[32] Taking open marine conditions as the starting point is not always valid in the application to the Late Miocene evolution of the Mediterranean. Here we consider t_{EQ} for the sequence of Late Miocene $^{87}Sr/^{86}Sr$–salinity steps as postulated by *Flecker et al.* [2002] (Figure 8a). This sequence consists of the following steps: the pre–MSC path starts at a salinity of 35–40 g/l and oceanic $^{87}Sr/^{86}Sr$ (situation termed F0), representing the main basins and sub-basins at normal marine conditions, and is followed by "F2" 35–40 g/l and 0.70875–0.7088, for the sub-basins deviating from the oceanic Sr isotope curve. The MSC evaporite path consists of "E0" (130–160 g/l and oceanic $^{87}Sr/^{86}Sr$) to represent the earliest gypsum precipitation, and "E1" (130–160 g/l and 0.70882–0.70887) to represent the Lower Evaporites that have $^{87}Sr/^{86}Sr$ outside the error envelope of coeval oceanic values (Figure 1). Figure 8b shows the evolution of $^{87}Sr/^{86}Sr$ and salinity between the aforementioned equilibrium states. It can be seen that most of the salinity and $^{87}Sr/^{86}Sr$ change required occurs relatively early in the process of full equilibration. We therefore chose to evaluate and compare the times at which $^{87}Sr/^{86}Sr$ and salinity have reached 95% of the total change required. For the three steps shown, F0 → F2, F2 → E0, and E0 → E1, this time is respectively 11.5, 18.5 and 71.5 kyr (Figure 8b). This implies that the response time of $^{87}Sr/^{86}Sr$ to changes in fR is rapid with unrestricted Atlantic exchange (F0 → F2) and slower with restriction (E0 → E1).

[33] It follows that, as long as the basin is not strongly restricted, the use of steady state solutions is valid since the time taken to reach a steady state is not more than the error on the precessional age-model and the average sampling resolution. However, when the basin is strongly restricted and the fresh water budget is close to zero, the time taken to move between steady states increases rapidly to 50 kyr and more. $^{87}Sr/^{86}Sr$-data at high restrictions and near-zero water budget can therefore only be considered as steady state solutions when time between them is long (>50 kyr) or when the rate of change in $^{87}Sr/^{86}Sr$ and/or salinity is small.

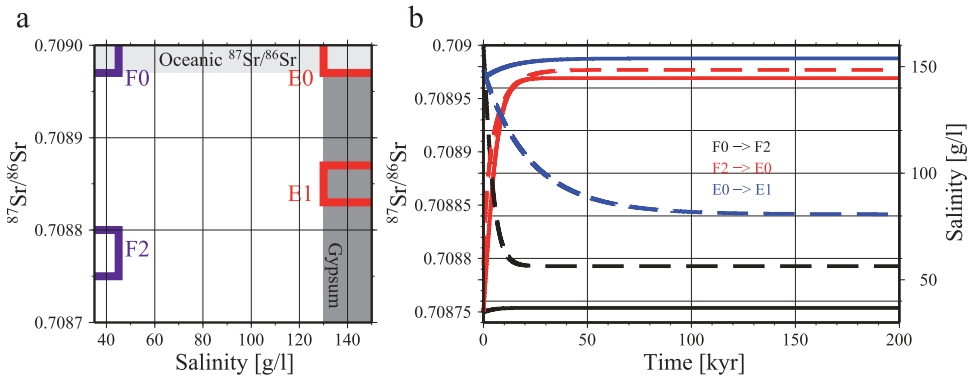

Figure 8. (a) The equilibrium states as defined by *Flecker et al.* [2002] in salinity-$^{87}Sr/^{86}Sr$ space. (b) Salinity (solid lines) and $^{87}Sr/^{86}Sr$ (dashed) evolution between these states.

5.2. The Pre-Evaporite Sequence

[34] Strontium ratios measured in Mediterranean Miocene-Pliocene sequences have the largest data density between 10–4.5 Ma (Figure 1). Application of the model is also limited to this time interval because of the Late Miocene water budget and paleogeography (volume and surface area) used. Regional deviations from oceanic values in $^{87}Sr/^{86}Sr$ data in this interval have been interpreted as indicating sub-basin formation [*Flecker et al.*, 2002]. Differences in $^{87}Sr/^{86}Sr$ between the sub-basins of Turkey, central Italy and the Tyrrhenian Sea show that there is no general trend in divergence from the ocean Sr curve discernible, which makes application of the model difficult. The salinity and $^{87}Sr/^{86}Sr$ ranges from the pre-MSC F0 and F2 delineate two areas in g_{WA}-fR space (Figure 9a). For the central Mediterranean area during the F0 period, the Sr isotope ratios within error of oceanic values do not allow to narrowly constrain fR, but the marine salinities mean that the gateway restriction has to be limited ($g_{WA} \geq 10^4$). Marginal basin sequences showing deviation from oceanic $^{87}Sr/^{86}Sr$ (F0 → F2), but no salinity change, move toward high fR with little gateway restriction. However, if we would plot F0 and F2 using the results of the model run with a smaller volume (Figure 6a) a more significant range of restrictions ($g_{WA} \geq 8 \cdot 10^2$) is found to be able to explain the data because small basins need more significant restriction before deviations from marine salinity and $^{87}Sr/^{86}Sr$ occur.

[35] The Southern Turkey and Italian sections all had a marginal position in the Late Miocene adjacent to the Taurides and Apennine orogens, respectively. It is therefore likely that they received runoff from these mountain ranges, including Sr from weathering and eroding the dominantly Mesozoic successions. If small basins have restricted exchange with Atlantic-like water, small changes in the volume of river input will have a large effect on the fR factor (since the reference value of R is also small) and hence on salinity and $^{87}Sr/^{86}Sr$ (Figure 6). Deviations from coeval Atlantic $^{87}Sr/^{86}Sr$ within these small marginal basins could therefore imply periods of localized increased river input. Given sampling density and the uncertainty in the age models used to date these sections, it is difficult to make detailed comparisons of their Sr isotope records. However, the tendency in the marginal basins to deviate from ocean values occurs for as long as the record we have. 8.3-6.5 Ma is a period of divergence in all marginal basins (Figure 1). Around 7.5 Ma, even central Mediterranean basin data plot

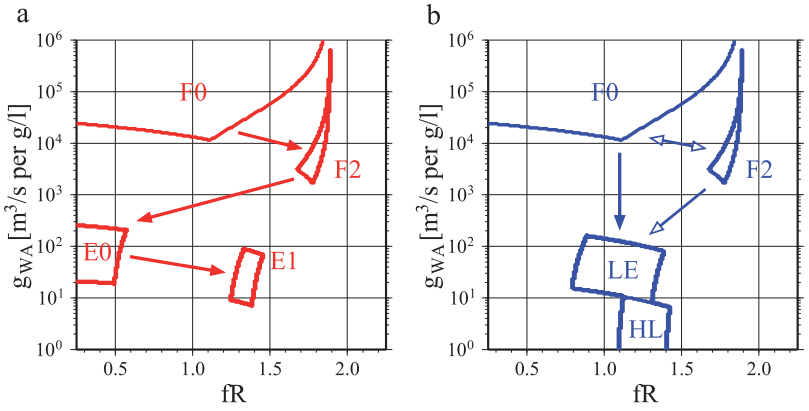

Figure 9. Diagram (a) shows the salinity-$^{87}Sr/^{86}Sr$ path from *Flecker et al.* [2002] in red. (b) Shows the path proposed in this study in blue, with the sub-basin path in open arrows. F0 indicates pre-MSC values in the central basins, F2 in the northern subbasins, E0 the onset of the MSC, and E1 the Lower Evaporites according to *Flecker et al.* [2002]. LE (Lower Evaporite gypsum) and HL (Lower Evaporite halite) are similar to the intervals in Figure 1.

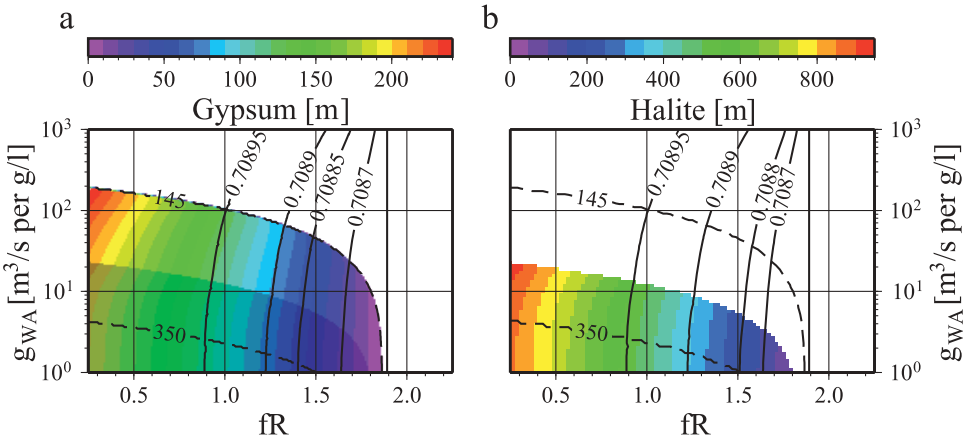

Figure 10. Diagrams shows (a) gypsum thickness deposited in 400 kyr as a function of river discharge (fR) and the Atlantic exchange coefficient g_{WA} for a 1 box model starting at normal marine conditions, the halite saturation domain is shaded; (b) halite thickness deposited in 80 kyr once a steady state is reached. R is expressed as a fraction, fR, of the reference value which is defined as the Late Miocene value from *Gladstone et al.* [2007]. Note how the vertical scale is logarithmic.

significantly lower than coeval ocean values, possible linked to the end of the Tortonian Salinity Crisis (7.6 Ma) [*Krijgsman et al.*, 2000] and the time at which the Rifian corridor reached its maximum depth [*Krijgsman et al.*, 1999b]. Around 6.8–6.5 Ma all data are within range of coeval seawater again. Hereafter, Tyrrhenian Sea and Southern Turkey data sets show another period of divergence while data from Pissouri diverge from the ocean curve shortly before onset of the MSC. The lack of major rivers around the Tyrrhenian Sea in combination with its size and $^{87}Sr/^{86}Sr$ gives rise to the question if river input is the $^{87}Sr/^{86}Sr$-lowering mechanism here. In the Tortonian, back-arc extension and rifting initiated the formation of the Tyrrhenian Sea as we know it today [*Kastens et al.*, 1988]. All samples from the Tyrrhenian sea are from an ODP core, and, certainly in deep water sections, basaltic volcanism and/or seafloor spreading could have been an important source of fluids with very low $^{87}Sr/^{86}Sr$.

5.3. Onset of the MSC

[36] Demonstrating the Sr isotope evolution during the salinity transition to gypsum precipitation at the beginning of the MSC is difficult because almost all sections with $^{87}Sr/^{86}Sr$ data start or end close to the onset of the LE. Combining available records of the central basins of the Mediterranean suggests that the change in $^{87}Sr/^{86}Sr$ is from Atlantic values of about 0.7090 to values in the range 0.70895–0.70885, with outliers on the ocean curve, while salinity increases from ~35 to >145 g/l. Connecting these two points in Figure 9b implies a change from a broad range of possible fR's with limited restriction ($g_{WA} \geq 10^4$) to fR lower than 1.4 with strong restriction ($g_{WA} \approx 10^2$). The required restriction may have resulted from the closure of the Rifian corridor (~6.0 Ma) [*Krijgsman et al.*, 1999b] and/or closure of parts of the Betic corridor, although some gateway must have persisted during LE deposition to supply salt [*Meijer and Krijgsman*, 2005] and, at the same time, limit evaporite thickness [*Meijer*, 2006; *Krijgsman and Meijer*, 2008].

[37] Whereas our model suggests simple gateway restriction as the MSC initiator, a transgression has been suggested by *Flecker et al.* [2002] (F2–E0, Figure 9a) based on the shift from low $^{87}Sr/^{86}Sr$ in some sub-basins (F2) to more oceanic values in the LE (E0). *Flecker et al.* [2002] interpreted an increase in their input parameter (defined as the inflow from the Atlantic over the sum of all incoming water) as an increase in Atlantic input, while their equations and our model show that this corresponds to an increase in E or decrease in R. Although using pre-MSC data from sub-basins and MSC data from central basins to infer a Mediterranean-wide transgression is questionable, this scenario can be tested with our model. To do this, the model, which contains the hypsometry of the Late Miocene Mediterranean (a look-up table is used to update volume and surface area when changing sea level), is forced to undergo a transgression from −100 to 0 m (with respect to the present-day sea level) at fR = 1.75, fE = 1 and $g_{WA} = 10^4$. Instead of the normal inflow parametrization, inflow linearly increases with time from a steady state value at −100 m to another steady state value at 0 m. The starting point is chosen to represent the sub-basin salinity and $^{87}Sr/^{86}Sr$ just before the MSC. Independent of the rate of sea level change the $^{87}Sr/^{86}Sr$ went up from 0.70885 to 0.70895, consistent with the proposed rise in sub-basin $^{87}Sr/^{86}Sr$. However, salinity increased only 4 g/l to 41.6 g/l, not even close to gypsum saturation. To the extent that assumptions and simplifications inherent to our model are correct, we can rule out a transgression as the only trigger for initial gypsum precipitation.

5.4. Evaporite Deposition

[38] The exchange parametrization used in our model is hard to combine with large sea level changes because volume conservation is assumed in the Mediterranean. Hence we can only study the deep water depositional scenario [*Krijgsman et al.*, 1999a] of the LE and halite. LE deposition took place in approximately 360 kyr, from 5.96 to 5.61 Ma [*Roveri et al.*, 2008]. A model-based estimate of the expected

gypsum thickness during LE deposition can be made by starting from open marine conditions and letting the model run for 400 kyr (40 kyr, the average time to gypsum saturation, + 360 kyr) for each combination of restriction and water budget. Thicknesses are given as homogeneous thickness over the total water covered area. The dominant control on gypsum thickness is fR, with increasing thickness occurring at lower fR values (Figure 10a). This is because when the Mediterranean water deficit is large, the volume of Atlantic inflow is substantial, importing large volumes of salt into the Mediterranean. The more subtle decrease in thickness controlled by increasing restriction (Figure 10a) is caused by the associated decrease in outflow which, through volume conservation, decreases the inflow and thus the input of salt. After crossing into halite saturation the rate of salinity increase drops due to precipitation of a larger percentage of the incoming salts.

[39] The majority (>90%) of $^{87}Sr/^{86}Sr$ values from LE deposits are between 0.70895 and 0.70885 (Figure 9b) which corresponds to g_{WA} and fR that yield gypsum thicknesses between 50 and 130 meter covering the whole Mediterranean basin (Figure 10a). If anoxic conditions in deep basins inhibited gypsum formation [*Manzi et al.*, 2007] this would probably have resulted in greater thicknesses precipitated in shallow water. A thickness increase by a factor 2–4 is a reasonable range to consider if gypsum formation takes place across only 25–50% of the Mediterranean. This increases the modeled thicknesses to 100–520 m. Observed gypsum thicknesses in the field have an average of 150 m [*CIESM*, 2008] with local variations (e.g., Vena del Gesso: 227 m [*Lugli et al.*, 2007]; Sorbas: 130 m [*Braga et al.*, 2006]).These relatively low observed thicknesses may indicate that gypsum precipitated across a relatively large area of basin floor and/or that most of the Mediterranean had a relatively low average $^{87}Sr/^{86}Sr$ during LE formation (higher fR) and/or that the preserved gypsum thickness is not the original thickness precipitated due to its vulnerability to erosion and dissolution on the basin margins. Massive halite formation (shaded area in Figure 10a) did not occur before 5.61 Ma, implying that the exchange parameter during LE gypsum formation was between 10^2 and $10^{0.8}$ $m^3/s/(g/l)$ (Figure 9b). This is in accord with results from a blocked outflow model which uses the present-day water budget [*Krijgsman and Meijer*, 2008]; the more severe restriction in our model results is the result of our use of a Late Miocene water budget.

[40] Between 5.61 and 5.53 Ma resedimented lower gypsum and halite were deposited in deep basins. Sea level certainly dropped at least once during halite deposition inhibiting outflow and limiting salt supply to the Mediterranean. Because our model does not change sea level, it overestimates the supply and deposition of salt when applied to this interval. Hence, by multiplying the sedimentation rate at equilibrium with the duration of halite formation, 80 kyr (Figure 10b), a maximum estimate of halite deposition can be acquired. For salinities above the 350 g/l contour the water deficit and decreasing inflow have the same effect on deposited halite thickness as described above for gypsum. Figure 10 seems to suggest that the start of halite formation does not coincide with the 350 g/l contour. Actually, halite formation is taken to start when the salinity reaches 350 g/l but for a range of fR and g_{WA} the ensuing balance between inflow, precipitation and outflow keeps the salinity constant at this critical value. This range is expressed by the color-contoured segment above the 350 g/l contour. Below the 350 g/l contour, salinity is higher than 350 g/l. Inflow and water deficit have the same control over halite thickness as they do over gypsum, however, accumulated halite thickness is also affected by the time taken to reach saturation which increases significantly at high restrictions and leaves less time for precipitation. This aspect is ignored here, however, because neither the initial conditions, nor the conditions at the end of the LE, can be sufficiently constrained.

[41] $^{87}Sr/^{86}Sr$ values during halite deposition range between 0.7089 and 0.7088 with values up to 0.70895 in east Mediterranean DSDP samples. Salt thicknesses in this $^{87}Sr/^{86}Sr$ range reach 200–370 m (Figure 10b), which corresponds to thicknesses of 700–1300 m if all halite is deposited in the much smaller area (28% of the Mediterranean) outlined by *Rouchy and Caruso* [2006]. By including the maximum of 0.70895 in the $^{87}Sr/^{86}Sr$ range (dashed range in Figure 9b), maximum thicknesses up to 2000 m can be achieved. Halite thicknesses in the deep basins inferred from seismics range from 600–1000 m in the western basin, including resedimented LE, and 1000–3500 m, with an average of 1500–2000 m, in the eastern Mediterranean [*Lofi et al.*, 2005]. The good agreement between model results and seismic observations confirms, again [*Meijer*, 2006; *Krijgsman and Meijer*, 2008], the viability of the blocked outflow scenario for halite deposition. But also shows that small outflows do not inhibit halite formation, but even slightly enhance the formation rate due to the larger salt supply. *Krijgsman and Meijer* [2008] found the halite thickness range inferred from seismics was on the low end of their modeled halite thickness range, while it is on the higher side of ours. This difference is the result of the larger fresh water input in the Late Miocene water budget with respect to the present-day budget used in earlier modeling research along with the unknown quantity of resedimented lower gypsum interbedded with the deep halite deposits.

6. Discussion

6.1. Uncertainties Inherent to the Model

[42] Implicit in our model set up and input are a few assumptions that have to be highlighted because they can be a source of uncertainty in the results. We assumed homogeneous water characteristics in each of the boxes, neglecting the likelihood of a stratified water column. In a stratified basin, salt is concentrated toward the bottom and Mediterranean outflow has salinities close to Atlantic values [*Meijer*, 2006]. If strontium is entirely independent of salinity, a strong stratification with respect to salinity may coexist with well-mixed, homogeneous $^{87}Sr/^{86}Sr$. This would lead to large deep water salinities with only minor restriction of gateway exchange and divergence of $^{87}Sr/^{86}Sr$ away from oceanic values because inflow decreases drastically as a result of limited density contrast and river input becomes more dominant.

[43] Our transgression experiment seemed to rule out a transgression as the only trigger for gypsum precipitation, but uncertainty in the distribution of strontium during periods of increased stratification leaves room for further investigation.

[44] In the outflow parametrization the density difference ($d\rho$) between the Mediterranean and Atlantic is a function of salinity only. The density difference can be expressed as

$$d\rho(S) = \rho_0\beta(S_W - S_A) \quad (1)$$

Including temperature, this becomes

$$d\rho(S,T) = \rho_0(\beta(S_W - S_A) - \alpha(T_W - T_A)) \quad (2)$$

where ρ_0 is a reference density, α and β are the thermal expansion and haline contraction coefficients of seawater and T_x and S_x are the temperatures and salinities of the Western Mediterranean and Atlantic. In seawater at 10°C and 35 g/l $\beta/\alpha \approx 5$ [*Feistel*, 2003], i.e. 1 g/l difference in salinity affects the $d\rho$ the same as 5°C. At present, the salinity difference (dS) between Atlantic and Mediterranean is ≈2 g/l with little temperature difference (dT). A dT of 1°C would introduce a percent error (δ) of 12.3% between $d\rho$ (S, T) and $d\rho$ (S) (Figure S2). Because outflow is proportional to $d\rho$, outflow in this example would be overestimated by 12.3% too. However, as illustrated in Figure S2, the error decreases significantly with increasing dS. At dS = 20 and dT = 1, dT = 2, and dT = 5, the error is only 1.1, 2.2 and 5.8%. During gypsum (dS > 95 g/l) and halite deposition (dS > 300 g/l), a dT of 5 results in, respectively, <1.2 and <0.4% error in the outflow calculation. α and β being functions of temperature and salinity, β/α can increase up to ≈2 at high temperature and salinity [*Feistel and Marion*, 2007]. Even with this increased temperature sensitivity, errors are never more than a few percent. Because our study focusses on relatively high salinity environments where temperature induced errors in the outflow are small, omitting temperature effects is justified.

[45] Not included in our model are sinks for Sr and changes in sea level, Atlantic $^{87}Sr/^{86}Sr$ and river discharge. [Sr] and salinity increase with the same factor as long as salt formation is ignored, while in reality sediments will take up Sr from the Mediterranean. Especially at the high evaporite sedimentation rates observed in the MSC this Sr-sink becomes important. The model is less sensitive to influxes of both river and oceanic waters if sedimentation is ignored, because a high Sr concentration enhances the buffer effect.

[46] Late Miocene sea level is on average similar to present-day [*Miller et al.*, 2005], but sea level fluctuations would affect the surface area of the Mediterranean, the amount of evaporation and the exchange with the Atlantic. Nevertheless, eustatic sea level changes are ignored in our model, because it complicates gateway exchange and imposes a timeframe on sensitivity experiments.

[47] Atlantic $^{87}Sr/^{86}Sr$ in our model is always 0.7090, the average during the MSC, although it increases steadily from 0.7089 to 0.7095 between 10 and 4.5 Ma (Figure 1). In the pre-MSC period the difference between $^{87}Sr/^{86}Sr_A$ and $^{87}Sr/^{86}Sr_R$ is smaller than modeled, leading to an overestimation of Atlantic influence on $^{87}Sr/^{86}Sr_M$; for the MSC it is the other way around, underestimation of Atlantic influence results in lower $^{87}Sr/^{86}Sr_M$. Using the precise $^{87}Sr/^{86}Sr_A$ values would slightly stretch the $^{87}Sr/^{86}Sr$ pattern in Figure 4b to lower fR for the pre-MSC and limit it to higher fR for the MSC.

6.2. Late Miocene Climate and River Discharge

[48] The generally high fR needed to explain the $^{87}Sr/^{86}Sr$-salinity evolution during the Late Miocene (Figure 9b) can indicate two things: (1) the water budget from *Gladstone et al.* [2007] overestimates E-P and/or (2) a constant source of fresh water has been ignored. E-P from *Gladstone et al.* [2007] is higher (1 m/yr) than E-P in more recent models for the Messinian (0.85 m/yr) [*Murphy et al.*, 2009] and Tortonian (0.55 m/yr) [*Schneck et al.*, 2010] suggesting the E-P we have used here may indeed be too high. With an E-P of ~0.55 m/yr, the Messinian evolution of $^{87}Sr/^{86}Sr$ and salinity can be explained without changing the river discharge. Greater rainfall over North Africa during the Late Miocene due to a shift in the ITCZ, which tends to be underestimated by AGCMs [*Gladstone et al.*, 2007, and references therein], could be another cause of the high fR. Underestimation of the increased precipitation over North Africa may be the source of fresh water missing in our model, affecting both the river discharge and E-P.

[49] Another possible source of fresh water can be found in Chad. Connections between the Sahabi river system (Libya) and the Chad basin in the Mio-Pliocene have been proposed on the basis of satellite imagery [*Griffin*, 2002, 2006; *Drake et al.*, 2008; *Paillou et al.*, 2009] and fossils [*Otero et al.*, 2009]. Like most GCMs the atmospheric model used by *Gladstone et al.* [2007] has a very simplistic surface hydrology and transports most precipitation (some goes into soil moisture) instantaneously from the drainage area to the river mouth. This means that evaporation over the rivers and Lake Chad is not taken into account and all discharges are overestimated. A minimum estimate of evaporation over Lake Chad can be found by taking the soil evaporation from their atmospheric model at the assumed position of the lake. More realistic estimates can be derived by looking at evaporation in the semi-enclosed Red Sea at the same latitude. The soil evaporation results in an estimate of 26% evaporation from Lake Chad, Red Sea evaporations result in 47–90%.

[50] To fit the box model results without invoking overestimation (underestimation) of E-P (R) in the atmospheric model, Lake Chad must have had a discharge of 31–56% (for fR range 1.5–1.89) of the modeled discharge. This is well within the range of Chad discharge with evaporation taken into account, implying that Lake Chad may have been an important source of fresh water in the Late Miocene at times it was connected to the Mediterranean via the Sahabi drainage basin. Water levels in Lake Chad are likely to have varied considerably in accordance with the precessional cycle and overflow into or a connection with the Sahabi rivers was most likely during precessional minima.

[51] Without Lake Chad, the Late Miocene eastern Mediterranean R is dominated by Nile discharge (80.8% of total input) and the western Mediterranean R by the Rhone (86%). In this situation it is valid to use their water characteristics for the whole input. However, when we assume that the Chad Basin was connected (periodically) to the Mediterranean and its discharge was 31–56% of the value from *Gladstone et al.* [2007], Nile discharge is only 40–52% of eastern Mediterranean R. The extremely low $^{87}Sr/^{86}Sr$ from the Nile is caused by extensive basaltic rocks in its drainage area. These are not observed in other North African

drainage basins, which would result in higher $^{87}Sr/^{86}Sr$ in their discharge. If the Nile was less dominant in the Late Miocene, a $^{87}Sr/^{86}Sr$ closer to oceanic values should be used for eastern Mediterranean river discharge. In our model this would result in a shift of the $^{87}Sr/^{86}Sr$ pattern toward higher fR; more river input is needed to deviate $^{87}Sr/^{86}Sr_M$ from oceanic values.

[52] Summarizing, the seemingly overestimated E-P and underestimated river discharge in the water budget from *Gladstone et al.* [2007] are either caused by underestimation of the effect of the shift in ITCZ or leaving out the Chad discharge. The general trend in climate is an decreasing E from Tortonian to Messinian with a possible inflow of water from the Chad basin during precession minima, improving conditions for sapropel formation and marl-gypsum cycles in the Mediterranean [*Köhler et al.*, 2010]. According to our model the most probable hydrological budget for the Late Miocene would be E-P in the range 0.67–0.85 m/yr, R between 0.63 and 0.8 m/yr (fR: 1.2–1.5; 3–4 times present-day values) and an even higher R during precession minima before the MSC.

7. Conclusions

[53] We developed a box model incorporating $^{87}Sr/^{86}Sr$ to examine the influence of gateway restriction, strontium characteristics of the input fluxes, climate and basin size/volume, on modeled $^{87}Sr/^{86}Sr$ and salinity values. With our time-dependent set of equations we have shown that the steady state assumption of previous studies regarding the $^{87}Sr/^{86}Sr$-salinity relationship is valid as long as either the basin is not strongly restricted and has a net water budget not close to zero, or when changes in $^{87}Sr/^{86}Sr$, restriction and water budget are slow with respect to the time taken to reach equilibrium. Sensitivity tests revealed that (1) in a model with the present-day water budget, contrary to a model with a Late Miocene budget, $^{87}Sr/^{86}Sr$ values in the Mediterranean will never significantly deviate from Atlantic values regardless of restriction and reasonable changes in the fresh water components of the budget, (2) the Mediterranean $^{87}Sr/^{86}Sr$ is most affected by uncertainty in $[Sr]_R$ and $^{87}Sr/^{86}Sr_R$ when the net fresh water budget is close to zero or/and gateway restriction is severe and (3) that the water budget of a small basin is dominated by exchange with the Atlantic up to more significant gateway restriction than that of a larger basin.

[54] The knowledge gained was applied to the Late Miocene salinity - $^{87}Sr/^{86}Sr$ record. The main conclusions and implications are the following:

[55] 1. $^{87}Sr/^{86}Sr$ data from pre-MSC sub-basins has only local significance; a comprehensive mechanism to explain all sub-basin data is lacking and central Mediterranean data generally do not show the same trends.

[56] 2. Onset of the MSC can be explained with a simple restriction of the gateway(s) between the Mediterranean and Atlantic. Also, the proposed transgression scenario can be rejected as the only trigger for initial gypsum precipitation on the basis of our model results.

[57] 3. Lower Evaporite gypsum formed in a basin with significantly less outflow than proposed by *Krijgsman and Meijer* [2008] because of the higher river input to the Mediterranean resulting from using a Late Miocene climate rather than present-day.

[58] 4. Halite thicknesses formed with the observed $^{87}Sr/^{86}Sr$ values between 5.61 and 5.53 Ma (700–1300 m) are on the low side of the observed thickness range (600–3500 m) because the large Late Miocene fresh water budget limits halite deposition rates and observed thicknesses from seismics are overestimated.

[59] Stemming from the discussion, we can also conclude that the most probable hydrological budget for the Late Miocene has E-P in the range 0.67–0.85 m/yr, R between 0.63 and 0.8 m/yr and an even higher R during precession minima prior to the MSC.

Appendix A: Model Equations

[60] The equations underlying the model are here given for the western Mediterranean in a 2-box model for the case of two-way exchange between Mediterranean and Atlantic (Figure 2). The linear parametrization of deep outflow between Atlantic and Mediterranean, similar for the western-eastern Mediterranean gateway, gives

$$Q_{WA} = g_{WA} \times (S_W - S_A) \tag{A1}$$

[61] The temporal change in total basin volume, which is always zero in the experiments presented in this paper, is given by

$$dV/dt = Q_{AW} - Q_{WA} + Q_{EW} - Q_{WE} + Q_R - Q_{EP} \tag{A2}$$

[62] The temporal changes in, respectively, salinity, strontium concentration and strontium ratio are given by

$$dS_W/dt = ((S_A - S_W)Q_{AW} + (S_E - S_W)Q_{EW} - S_W Q_R + S_W Q_{EP})/V_W \tag{A3}$$

$$d[Sr]_W/dt = \left(\left([Sr]_A - [Sr]_W\right)Q_{AW} + \left([Sr]_E - [Sr]_W\right)Q_{EW} - \left([Sr]_R - [Sr]_W\right)Q_R + [Sr]_W Q_{EP}\right)/V_W \tag{A4}$$

$$dR_W/dt = \left((R_A - R_W)[Sr]_A Q_{AW} + (R_E - R_W)[Sr]_E Q_{EW} + (R_R - R_W)[Sr]_R Q_R\right)/\left(V_W [Sr]_W\right) \tag{A5}$$

[63] Where R_x is an abbreviation of $^{87}Sr/^{86}Sr_x$. The inflows appearing in equations (A3)–(A5) are replaced, using equation (A2), by a combination of outflows and fresh water fluxes. The resulting coupled ordinary differential equations are solved using the second-order Runge-Kutta method.

[64] **Acknowledgments.** The authors acknowledge useful discussions with Pasha Karami and Iuliana Vasiliev. We would like to thank Dan Lunt for supplying us with evaporation data from the AGCM and an anonymous referee, Matt Fantle, and the editor for their constructive comments. Figures in this paper were created using GMT version 4.1.2

[*Wessel and Smith*, 1991]. RPMT is supported by the Netherlands Research Centre of Integrated Solid Earth Science (ISES).

References

Albarède, F., and A. Michard (1987), Evidence for slowly changing $^{87}Sr/^{86}Sr$ in runoff from freshwater limestones of southern France, *Chem. Geol.*, *64*, 55–65.

Bassetti, M., V. Manzi, S. Lugli, M. Roveri, A. Longinelli, F. Lucchi, and M. Barbieri (2004), Paleoenvironmental significance of Messinian post-evaporitic lacustrine carbonates in the northern Apennines, Italy, *Sediment. Geol.*, *17*, 1–18.

Benson, R., K. Rakic-El Bied, and G. Bonaduce (1991), An important current reversal (influx) in the Rifian corridor (Morocco) at the Tortonian-Messinian boundary: The end of the Tethys ocean, *Paleoceanography*, *6*(1), 164–192.

Betzler, C., J. Braga, J. Martín, I. Sánchez-Almazo, and S. Lindhorst (2006), Closure of a seaway: Stratigraphic record and facies (Guadix basin, Southern Spain), *Int. J. of Earth Sciences*, *95*, 903–910.

Blanc, P.-L. (2006), Improved modelling of the Messinian Salinity Crisis and conceptual implications, *Palaeogeogr. Palaeoclimatol. Palaeoecol.*, *238*, 349–372.

Braga, J., J. Martín, R. Riding, J. Aguirre, I. Sánchez-Almazo, and J. Dinarès-Turell (2006), Testing models for the Messinian salinity crisis: The Messinian record in Almería, SE Spain, *Sediment. Geol.*, *188–189*, 131–154.

Brass, G. (1976), The variation of the marine $^{87}Sr/^{86}Sr$ ratio during Phanerozoic time: interpretation using a flux model, *Geochim. Cosmochim. Acta*, *40*, 721–730.

Broecker, W., and T.-H. Peng (1982), *Tracers in the Sea*, Columbia Univ., Palisades, New York.

CIESM (2008), *The Messinian Salinity Crisis from mega-deposits to microbiology–A consensus report*, *CIESM Workshop Monogr.*, vol. 33, edited by F. Briand, 168 pp., CIESM, Monaco.

Drake, N., A. El-Hawat, P. Turner, S. Armitage, M. Salem, K. White, and S. McLaren (2008), Palaeohydrology of the Fazzan Basin and surrounding regions: The last 7 million years, *Palaeogeogr. Palaeoclimatol. Palaeoecol.*, *263*, 131–145.

Feistel, R. (2003), A new extended Gibbs thermodynamic potential of seawater, *Prog. Oceanogr.*, *58*, 43–114.

Feistel, R., and G. Marion (2007), A Gibbs-Pitzer function for high-salinity seawater thermodynamics, *Prog. Oceanogr.*, *74*, 515–539.

Flecker, R., and R. Ellam (1999), Distinguishing climatic and tectonic signals in the sedimentary successions of marginal basins using Sr isotopes: An example from the Messinian salinity crisis, Eastern Mediterranean, *J. Geol. Soc.*, *156*, 847–854.

Flecker, R., and R. Ellam (2006), Identifying Late Miocene episodes of connection and isolation in the Mediterranean-Paratethyan reals using Sr isotopes, *Sediment. Geol.*, *188–189*, 189–203.

Flecker, R., S. de Villiers, and R. Ellam (2002), Modelling the effect of evaporation on the salinity-$^{87}Sr/^{86}Sr$ relationship in modern and ancient marginal-marine systems: The Mediterranean Messinian Salinity Crisis, *Earth Planet. Sci. Lett.*, *203*, 221–233.

Fortuin, A., J. Kelling, and T. Roep (1995), The enigmatic Messinian–Pliocene section of Cuevas del Almanzora (Vera Basin, Spain) revisited–Erosional features and strontium isotope ages, *Sediment. Geol.*, *97*, 177–201.

Gladstone, R., R. Flecker, P. Valdes, D. Lunt, and P. Markwick (2007), The Mediterranean hydrologic budget from a Late Miocene global climate simulation, *Palaeogeogr. Palaeoclimatol. Palaeoecol.*, *251*, 254–267.

Goudie, A. (2005), The drainage of Africa since the Cretaceous, *Geomorphology*, *67*, 437–456.

Govers, R., P. Meijer, and W. Krijgsman (2009), Regional isostatic response to Messinian Salinity Crisis events, *Tectonophysics*, *463*, 109–129.

Griffin, D. (2002), Aridity and humidity: Two aspects of the late Miocene climate of North Africa and the Mediterranean, *Palaeogeogr. Palaeoclimatol. Palaeoecol.*, *182*, 65–91.

Griffin, D. (2006), The late Neogene Sahabi rivers of the Sahara and their climatic and environmental implications for the Chad basin, *J. Geol. Soc.*, *163*, 905–921.

Hodell, D., G. Mead, and P. Mueller (1990), Variation in the strontium isotopic composition of seawater (8 Ma to present): Implications for chemical weathering rates and dissolved fluxes to the oceans, *Chem. Geol.*, *80*, 291–307.

Hsü, K., W. Ryan, and M. Cita (1973), Late Miocene desiccation of the Mediterranean, *Nature*, *242*, 240–244.

Hüsing, S., O. Oms, J. Agustí, M. Garcés, T. Kouwenhoven, W. Krijgsman, and W.-J. Zachariasse (2010), On the late Miocene closure of the Mediterranean–Atlantic gateway through the Guadix basin (southern Spain), *Palaeogeogr. Palaeoclimatol. Palaeoecol.*, *291*, 167–179.

Kastens, K., et al. (1988), ODP Leg 107 in the Tyrrhenian Sea: Insights into passive margin and back-arc basin evolution, *Geol. Soc. Am. Bull.*, *100*, 1140–1156.

Keogh, S., and R. Butler (1999), The Mediterranean water body in the late Messinian: interpreting the record from marginal basins on Sicily, *J. Geol. Soc.*, *156*, 837–846.

Köhler, C., D. Heslop, W. Krijgsman, and M. Dekkers (2010), Late Miocene paleoenvironmental changes in North Africa and the Mediterranean recorded by geochemicalproxies (Monte Gibliscemi section, Sicily), *Palaeogeogr. Palaeoclimatol. Palaeoecol.*, *285*, 66–73.

Kouwenhoven, T., and G. van der Zwaan (2006), A reconstruction of late Miocene Mediterranean circulation patterns using benthic foraminifera, *Palaeogeogr. Palaeoclimatol. Palaeoecol.*, *238*, 373–385.

Kouwenhoven, T., F. Hilgen, and G. van der Zwaan (2003), Late Tortonian–early Messinian stepwise disruption of the Mediterranean–Atlantic connections: constraints from benthic foraminiferal and geochemical data, *Palaeogeogr. Palaeoclimatol. Palaeoecol.*, *198*, 303–319.

Krijgsman, W., and P. Th. Meijer (2008), Depositional environments of the Mediterranenan "Lower Evaporites" of the Messinian salinity crisis: Constraints from quantitative analysis, *Mar. Geol.*, *253*, 73–81.

Krijgsman, W., F. Hilgen, I. Raffi, F. Sierro, and D. Wilson (1999a), Chronology, causes and progression of the Messinian Salinity Crisis, *Nature*, *400*, 652–655.

Krijgsman, W., C. Langereis, W. Zachariasse, M. Boccaletti, G. Moratti, R. Gelati, S. Iaccarino, G. Papani, and G. Villa (1999b), Late Neogene evolution of the Taza-Guercif basin (Rifian corridor, Morocco) and implications for the Messinian salinity crisis, *Mar. Geol.*, *153*, 147–160.

Krijgsman, W., M. Garcés, J. Agustí, I. Raffi, C. Taberner, and W. Zachariasse (2000), The 'Tortonian salinity crisis' of the eastern Betics (Spain), *Earth Planet. Sci. Lett.*, *181*, 497–511.

Leeder, M. (1999), *Sedimentology and Sedimentary Basins: From Turbulence to Tectonics*, 592 pp., Blackwell Sci., Malden, Mass.

Lofi, J., C. Gorini, S. Berné, G. Clauzon, A. T. D. Reis, W. Ryan, and M. Steckler (2005), Erosional processes and paleo-environmental changes in the Western Gulf of Lions (SW France) during the Messinian Salinity Crisis, *Mar. Geol.*, *217*, 1–30.

Lugli, S., M. Bassetti, V. Manzi, M. Barbieri, A. Longinelli, and M. Roveri (2007), The Messinian 'Vena del Gesso' evaporites revisited: Characterization of isotopic composition and organic matter, in *Evaporiates Through Space and Time*, edited by B. C. Schreiber, S. Lugli, and M. Bąçbel, *Geol. Soc. Spec. Publ.*, *285*, 179–190.

Manzi, V., et al. (2007), The deep–water counterpart of the Messinian Lower Evaporites in the Apennine foredeep: The Fanantello section (Northern Apennines, Italy), *Palaeogeogr. Palaeoclimatol. Palaeoecol.*, *251*, 470–499.

Mariotti, A., M. Struglia, N. Zeng, and K.-M. Lau (2002), The hydrological cycle in the Mediterranean region and implications for the water budget of the Mediterranean Sea, *J. Clim.*, *15*, 1674–1690.

Martín, J., J. Braga, J. Aguirre, and A. Puga-Bernabéu (2009), History and evolution of the North-Betic Strait (Prebetic Zone, Betic Cordillera): A narrow, early Tortonian, tidal–dominated, Atlantic–mediterranean marine passage, *Sediment. Geol.*, *216*, 80–90.

Matano, F., M. Barbieri, S. D. Nocera, and M. Torre (2005), Stratigraphy and strontium geochemistry of Messinian evaporite-bearing successions of the southern Apennines foredeep, Italy: implications for the Mediterranean "salinity crisis" and regional palaeogeography, *Palaeogeogr. Palaeoclimatol. Palaeoecol.*, *217*, 87–114.

McArthur, J., R. Howarth, and T. Bailey (2001), Strontium isotope stratigraphy: LOWESS version 3: best fit to the marine Sr-isotope curve for 0–509 Ma and accompanying look-up table for deriving numerical age, *J. Geol.*, *109*, 155–170.

McCullogh, M., and P. D. Dekker (1989), Sr isotope constraints on the mediterranean environment at the end of the Messinian salinity crisis, *Nature*, *342*, 62–65.

McKenzie, J., D. Hodell, P. Mueller, and D. Mueller (1988), Application of strontium isotopes to late Miocene–early Pliocene stratigraphy, *Geology*, *16*, 1022–1025.

Meijer, P. Th. (2006), A box model of the blocked-outflow scenario for the Messinian Salinity Crisis, *Earth Planet. Sci. Lett.*, *248*, 486–494.

Meijer, P. Th., and W. Krijgsman (2005), A quantitative analysis of the desiccation and re-filling of the Mediterranean during the Messinian Salinity Crisis, *Earth and Planet. Sci. Lett.*, *240*, 510–520.

Meijer, P. Th., R. Slingerland, and M. Wortel (2004), Tectonic control on past circulation of the Medittanean Sea: A model study of the Late Miocene, *Paleoceanography*, *19*, PA1026, doi:10.1029/2003PA000956.

Miller, K., M. Komnz, J. Browning, J. Wright, G. Mountain, M. Katz, P. Sugarman, B. Cramer, N. Christie-Blick, and S. Pekar (2005), The Phanerozoic record of global sea-level change, *Science*, *310*, 1293–1298.

Montanari, A., et al. (1997), Integrated stratigraphy of the Middle to Upper Miocene pelagic sequence of the Conero Riviera (Marche Region, Italy), in *Miocene Stratigraphy: An Integrated Approach*, edited by A. Montanari, G. Odin, and R. Coccioni, pp. 409–450, Elsevier Sci., Amsterdam.

Müller, D. (1993), Pliocene transgression in the western Mediterranean Sea: strontium isotopes from Cuevas del Almanzora (SE Spain), *Paleoceanography*, *8*, 127–134.

Müller, D., and P. Mueller (1991), Origin and age of the Mediterranean Messinian evaporites: implications from Sr isotopes, *Earth and Planet. Sci. Lett.*, *107*, 1–12.

Müller, D., P. Mueller, and A. McKenzie (1990), Strontium isotopic ratios as fluid tracers in Messinian evaporites of the Tyrrhenian Sea (western Mediterranean Sea), in *Tyrrhenian Sea: Sites 650–656*, *Proc. Ocean Drill. Program Sci. Results*, *107*, 603–614.

Murphy, L., D. Kirk-Davidoff, N. Mahowald, and B. Otto-Bliesner (2009), A numerical study of the climate response to lowered Mediterranean sea level during the Messinian Salinity Crisis, *Palaeogeogr. Palaeoclimatol. Palaeoecol.*, *279*, 41–59.

Otero, O., A. Pinton, H. T. Mackaye, A. Likius, P. Vignaud, and M. Brunet (2009), Fishes and palaeogeography of the African drainage basins: Relationships between Chad and neighbouring basins throughout the Mio-Pliocene, *Palaeogeogr. Palaeoclimatol. Palaeoecol.*, *274*, 134–139.

Paillou, P., M. Schuster, S. Tooth, T. Farr, A. Rosenqvist, S. Lopez, and J.-M. Melzieux (2009), Mapping of the major paleodrainage system in eastern Libya using orbital imaging radar: The Kufrah River, *Earth Planet. Sci. Lett.*, *277*, 327–333.

Palmer, M., and J. Edmond (1989), The strontium isotope budget of the modern ocean, *Earth Planet. Sci. Lett.*, *92*, 11–26.

Reinhardt, E., D. Stanley, and R. Patterson (1998), Strontium isotopic-paleontological method as a high-resolution paleosalinity tool for lagoonal environments, *Geology*, *26*, 1003–1006.

Rouchy, J., and A. Caruso (2006), The Messinian salinity crisis in the Mediterranean basin: A reassessment of the data and an integrated scenario, *Sediment. Geol.*, *188–189*, 35–67.

Roveri, M., S. Lugli, V. Manzi, and B. Schreiber (2008), The Messinian Sicilian stratigraphy revisited: new insights for the Messinian salinity crisis, *Terra Nova*, *20*, 483–488.

Schneck, R., A. Micheels, and V. Mosbrugger (2010), Climate modelling sensitivity experiments for the Messinian Salinity Crisis, *Palaeogeogr. Palaeoclimatol. Palaeoecol.*, *286*, 149–163.

Seidenkrantz, M.-S., T. Kouwenhoven, F. Jorissen, N. Shackleton, and G. van der Zwaan (2000), Benthic foraminifera as indicators of changing Mediterranean–Atlantic water exchange in the late Miocene, *Mar. Geol.*, *163*, 387–407.

Sprovieri, M., M. Barbieri, A. Bellanca, and R. Neri (2003), Astronomical tuning of the Tortonian $^{87}Sr/^{86}Sr$ curve in the Mediterranean basin, *Terra Nova*, *15*, 29–35.

Vasiliev, I., G.-J. Reichart, G. Davies, W. Krijgsman, and M. Stoica (2010), Strontium isotope ratios of the Eastern Paratethys during the Mio–Pliocene transition; Implications for interbasinal connectivity, *Earth Planet. Sci. Lett.*, *292*, 123–131.

Warren, J. (2006), *Evaporites: Sediments, Resources and Hydrocarbons*, Springer, New York.

Wessel, P., and W. Smith (1991), Free software helps map and display data, *EOS Trans. AGU*, *72*(41), 441.

R. Flecker, BRIDGE, School of Geographical Sciences, Bristol University, University Road, Bristol BS8 ISS, UK.

P. Th. Meijer, R. P. M. Topper, and M. J. R. Wortel, Department of Earth Sciences, Faculty of Geosciences, Utrecht University, Budapestlaan 4, NL-3584 CD Utrecht, Netherlands. (topper@geo.uu.nl)